Commun. Comput. Phys.
doi: 10.4208/cicp.171011.190712a

Vol. **14**, No. 1, pp. 153-173
July 2013

A Lattice Boltzmann and Immersed Boundary Scheme for Model Blood Flow in Constricted Pipes: Part 2 – Pulsatile Flow

S. C. Fu*, R. M. C. So and W. W. F. Leung

Department of Mechanical Engineering, The Hong Kong Polytechnic University, Hung Hom, Hong Kong.

Received 17 October 2011; Accepted (in revised version) 18 July 2012

Communicated by Kazuo Aoki

Available online 30 October 2012

Abstract. One viable approach to the study of haemodynamics is to numerically model this flow behavior in normal and stenosed arteries. The blood is either treated as Newtonian or non-Newtonian fluid and the flow is assumed to be pulsating, while the arteries can be modeled by constricted tubes with rigid or elastic wall. Such a task involves formulation and development of a numerical method that could at least handle pulsating flow of Newtonian and non-Newtonian fluid through tubes with and without constrictions where the boundary is assumed to be inelastic or elastic. As a first attempt, the present paper explores and develops a time-accurate finite difference lattice Boltzmann method (FDLBM) equipped with an immersed boundary (IB) scheme to simulate pulsating flow in constricted tube with rigid walls at different Reynolds numbers. The unsteady flow simulations using a time-accurate FDLBM/IB numerical scheme is validated against theoretical solutions and other known numerical data. In the process, the performance of the time-accurate FDLBM/IB for a model blood flow problem and the ease with which the no-slip boundary condition can be correctly implemented is successfully demonstrated.

AMS subject classifications: 76Z05, 76M20, 65M06

Key words: Finite difference method, lattice Boltzmann method, immersed boundary method, blood flow, constricted pipe.

1 Introduction

It was pointed out in a companion paper [1] that a viable numerical solver for blood flow modeling should at least be able to correctly simulate certain key features of blood flow. The more important of these are non-Newtonian fluid, incompressible pulsating

*Corresponding author. *Email addresses:* mescfu@ust.hk (S. C. Fu), mmmcso@polyu.edu.hk (R. M. C. So), Wallace.Leung@inet.polyu.edu.hk (W. W. F. Leung)

flow that could become erratic, three-dimensional (3-D) flow with complex and changing boundaries, and flow-structure interaction resulting from elastic wall boundary. In an attempt to develop an alternative numerical solver based on the lattice Boltzmann method (LBM), Fu and his co-workers [2–6] used their previously developed finite difference lattice Boltzmann method (FDLBM) as base to further extend the FDLBM to handle complex boundary by incorporating the immersed boundary method [7, 8] to their FDLBM; thus giving a combined FDLBM/IB numerical scheme [1] where the no-slip boundary condition is just as easy to implement as any other finite difference scheme used to solve the Navier-Stokes (NS) equations. This extension retains the ease with which the FDLBM can still perform computations using Cartesian grids in problems with complex boundaries. The FDLBM [2] can correctly resolve incompressible flow [3]; replicate Newtonian and non-Newtonian flow in microchannel and microtube accurately [2]; simulate incompressible flow with random variations in viscosity and pressure in channel/pipe [4]; and model 2-D and 3-D buoyant flow [5, 6]. Therefore, the FDLBM/IB is not only suitable for flow with complex boundary, but is also appropriate for incompressible Newtonian and non-Newtonian flow with external body force, and with random variation of viscosity and pressure.

With these successes, Fu et al. [1] adopted their FDLBM/IB numerical scheme to study steady Newtonian flow in constricted tubes at different Reynolds numbers. The resulting governing equations in the FDLBM/IB scheme are still linear, so they can be solved locally, explicitly and efficiently using Cartesian grids. The numerical scheme was further used to investigate Newtonian and non-Newtonian fluid flow in stenosed arteries and the effect of viscous stress and resistance on disordered flow patterns resulting from the constriction [1]. Their study brought closer to reality the development of LBM as an alternative to numerically solving the NS equations for blood flow simulation. However, the FDLBM and FDLBM/IB [1–6] developed to-date can only handle steady flow with and without random fluctuations. Therefore, its extension to unsteady flow in an axisymmetric domain would represent another forward step to render the method appropriate for blood flow simulation. The next step in the development of an LBM solver for blood flow modeling is to build on the steady FDLBM/IB experience [1], and extend the methodology to unsteady and pulsating flow. This necessitates the extension of the steady FDLBM and FDLBM/IB algorithms to time-accurate FDLBM and FDLBM/IB schemes.

The present paper reports on just this development. After validating the time-accurate FDLBM and FDLBM/IB scheme, numerical simulations of a modeled blood flow problem, namely that of Newtonian and non-Newtonian fluid flow in constricted tubes, using the time-accurate FDLBM/IB scheme are investigated and discussed.

2 The FDLBM/IB numerical scheme

A schematic representation of the blood flow problem, modeled by an incompressible flow through a rigid tube with a localized constriction, is shown in Fig. 1. In this model,

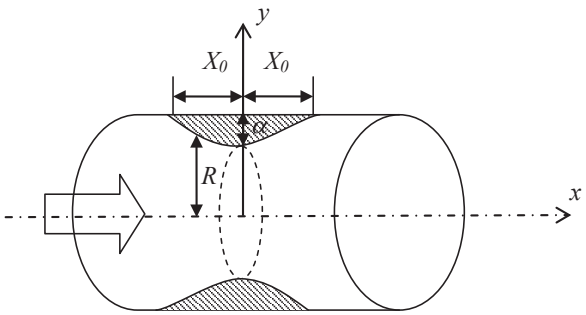

Figure 1: Schematic diagram of the model problem investigated.

axial symmetry as assumed in [9,10] is adopted. Since unsteady flow is considered, time dependent form of the NS equations and the associated lattice Boltzmann equations are presented below. All equations shown are normalized by appropriate reference parameters. Details of the relevant equations have been given previously [1–6]. Therefore, there is no need to go through this derivation again. On the other hand, details of the pseudo-time approach to solve the unsteady FDLBM will be discussed in the next section. Here, for the sake of completeness, a brief description of the governing unsteady NS equations and physical boundary conditions of the constricted tube flow, the associated FDLBM equations, and how the IB method can be implemented into the FDLBM is given.

2.1 Governing equations and physical boundary conditions

For the present problem, the effect of swirl behind the constriction is neglected [9,10]. The through flow rate is $\hat{Q}=\pi\hat{R}_0^2\hat{U}_0/2$ and the Reynolds number is given by $\mathrm{Re}=\hat{\rho}_0\hat{U}_0\hat{R}_0/\hat{\mu}_0$, where $\hat{R}_0$ is the unconstricted tube radius, $\hat{U}_0$ is the centerline velocity of a fully developed steady Poiseuille flow, $\hat{\rho}_0$ is fluid density and $\hat{\mu}_0$ is fluid viscosity. All dimensional quantities are represented by a 'hat'; their dimensionless counterparts are without a "hat". The subscript "0" is used to denote reference state. The dimensionless equations in cylindrical coordinates are given as

$$\frac{\partial\rho}{\partial t}+\frac{\partial\rho u}{\partial x}+\frac{\partial\rho v}{\partial y}+\frac{\rho v}{y}=0, \tag{2.1a}$$

$$\frac{\partial\rho u}{\partial t}+\frac{\partial\rho u^2}{\partial x}+\frac{\partial\rho uv}{\partial y}+\frac{\rho uv}{y}=-\frac{\partial p}{\partial x}+\frac{\partial\tau_{xx}}{\partial x}+\frac{\partial\tau_{xy}}{\partial y}+\frac{\tau_{xy}}{y}, \tag{2.1b}$$

$$\frac{\partial\rho v}{\partial t}+\frac{\partial\rho uv}{\partial x}+\frac{\partial\rho v^2}{\partial y}+\frac{\rho v^2}{y}=-\frac{\partial p}{\partial y}+\frac{\partial\tau_{xy}}{\partial x}+\frac{\partial\tau_{yy}}{\partial y}+\frac{\tau_{yy}}{y}, \tag{2.1c}$$

where

$$\tau_{xx}=\frac{2}{\mathrm{Re}}\frac{\partial u}{\partial x},\qquad \tau_{yy}=\frac{2}{\mathrm{Re}}\frac{\partial v}{\partial y},\qquad \tau_{xy}=\frac{1}{\mathrm{Re}}\left(\frac{\partial u}{\partial y}+\frac{\partial v}{\partial x}\right). \tag{2.2}$$

In these equations, all variables are normalized by their respective reference quantities, such that,

$$t=\frac{\hat{t}}{\hat{T}},\qquad (x,y)=\frac{(\hat{x},\hat{y})}{\hat{R}_0},\qquad (u,v)=\frac{(\hat{u},\hat{v})}{\hat{U}_0}, \tag{2.3a}$$

$$\rho=\frac{\hat{\rho}}{\hat{\rho}_0},\qquad p=\frac{\hat{p}}{\hat{\rho}_0\hat{U}_0^2},\qquad \left(\tau_{xx},\tau_{xy},\tau_{yy}\right)=\frac{\left(\hat{\tau}_{xx},\hat{\tau}_{xy},\hat{\tau}_{yy}\right)}{\hat{\rho}_0\hat{U}_0^2}. \tag{2.3b}$$

Here, (x,y) are the axial and radial coordinates, (u,v) are the axial and radial velocity components along x and y, respectively, t is time and p is pressure. The characteristic time $\hat{T}$ can be defined as $\hat{T}=\hat{R}_0/\hat{U}_0$ in the absence of external forcing. The unsteady, compressible form is used here because a pressure correction method is used to iterate for the incompressible solution (where $\rho=$constant is specified) and pulsating flows are considered. Thus, for steady incompressible flow, $\rho=$constant is recovered at steady state; the corresponding governing equations reduced to those given in [1]. The constriction geometry (Fig. 1) is described by a cosine curve using α_1 and X_0 to characterize the constant length and degree of occlusion, respectively [9,10],

$$R(x)=1-\frac{\alpha_1}{2}\left[1+\cos\left(\frac{\pi x}{X_0}\right)\right],\qquad -X_0\le x\le X_0, \tag{2.4a}$$

$$R(x)=1,\qquad |x|\ge X_0. \tag{2.4b}$$

2.2 FDLBM/IB numerical scheme

The FDLBM/IB has been discussed in detail previously [1]; it shows that the modeled lattice Boltzmann equation can recover the steady form of Eqs. (2.1)-(2.2) exactly. Here, for the sake of completeness, only the lattice Boltzmann equation (LBE) and other relevant equations are given below. The LBE is

$$\frac{\partial f_\alpha}{\partial t}+\vec{\xi}_\alpha\cdot\nabla f_\alpha+g_\alpha=-\frac{1}{\varphi}(f_\alpha-{f_\alpha}^{eq}), \tag{2.5}$$

where the lattice distribution function f_α and others to be defined later are normalized by $\hat{\rho}_0$, such that $f_\alpha=\hat{f}_\alpha/\hat{\rho}_0$, and α is an index used to denote the velocity lattice. The lattice model employed is a D2Q9 model; the expression of the equilibrium distribution function ${f_\alpha}^{eq}$ and its associated coefficients can be found in [1]. Besides f_α, another distribution function g_α is added to help recover the source terms in Eqs. (2.1a)-(2.1c). To implement the IB method into the FDLBM, an additional external body force is included in the NS equations through g_α. The macroscopic variables are determined from

$$\rho u=\sum_{\alpha=0}^{8}f_\alpha\xi_{\alpha x},\qquad \rho v=\sum_{\alpha=0}^{8}f_\alpha\xi_{\alpha y}, \tag{2.6a}$$

$$p=\sum_{\alpha=0}^{8}f_\alpha\frac{1}{2}\left(\xi_{\alpha x}^2+\xi_{\alpha y}^2\right)-\frac{1}{2}\rho\left(u^2+v^2\right)+\frac{\tau_{xx}+\tau_{yy}}{2}. \tag{2.6b}$$

Numerically, Eqs. (2.5)-(2.6) are solved using a splitting method (see [1–4]). The first step is to solve Eq. (2.5) by setting its right hand side to zero. This solution is used as the initial condition for the second step which is to solve the diffusion equation obtained by neglecting the advective term in Eq. (2.5). The scheme [1–4] is designed for steady flow, so the time variable in the equations is considered as a pseudo-time and the previous two procedures are repeated and iterated on the pseudo-time until the following criterion is satisfied,

$$\max\left\|\partial\left(p+\frac{1}{2}\rho\left(u^2+v^2\right)-\frac{\tau_{xx}+\tau_{yy}}{2}\right)\right\|\leq\frac{\Delta t^2\sigma^2}{2}, \tag{2.7}$$

thus ensuring that the continuity equation is determined to an error of $\mathcal{O}(\Delta t)$. The operator '∂' denotes the difference between successive time steps and the maximum norm is taken within the whole spatial domain. The numerical parameter σ can be a constant or allowed to vary for each iteration step according to

$$\sigma=c\sqrt{\max\left\|u^2+v^2+\frac{2p-\tau_{xx}-\tau_{yy}}{\rho}\right\|}. \tag{2.8}$$

Numerical experiments show that the scheme will become unstable if the choice of c is too small; however, it affects the convergence and accuracy if c is too large, so a small enough c for stable calculation is required for all simulation cases attempted in this paper. Further discussion of the convergence criterion for unsteady flow is given below.

3 Pseudo-time approach for time-accurate FDLBM

Most numerical schemes designed for solving unsteady incompressible NS equations adopt either the artificial compressibility or the pressure correction method. Both methods are made time accurate by treating the time-dependent terms in pseudo time. Real physical time terms are added in the governing equations and the solution is iterated to a pseudo-time convergence at each real physical time step. When the pseudo-time terms vanish, the solution obtained satisfies the complete time-dependent equations. For the sake of brevity, this approach is denoted as the pseudo-time approach. Detailed discussion of this approach can be found in [13]. The same approach is used to extend the steady FDLBM [2] to a time-accurate FDLBM. For illustration purpose, only the formulation for the time-accurate FDLBM is given here; its extension to a time-accurate FDLBM/IB is straightforward and will not be elaborated further.

For illustration purpose, it is only necessary to consider the Cartesian form of Eq. (2.5), i.e., the form with $g_\alpha=0$. In order to accomplish the objective of extending the steady FDLBM [2] to a time-accurate scheme using the pseudo-time approach, a real, physical time term is added as a body force, F_α, to Eq. (2.5) with $g_\alpha=0$. The equation can then be written as

$$\frac{\partial f_\alpha}{\partial t}+\xi_\alpha\cdot\nabla_{\vec{x}}f_\alpha+F_\alpha=-\frac{1}{\varphi}\left(f_\alpha-f_\alpha^{eq}\right), \tag{3.1}$$

such that

$$\sum_{\alpha=0}^{8} F_\alpha = \frac{\partial \rho}{\partial t'}, \qquad \sum_{\alpha=0}^{8} F_\alpha \xi_{\alpha x} = \frac{\partial \rho u}{\partial t'}, \tag{3.2a}$$

$$\sum_{\alpha=0}^{8} F_\alpha \xi_{\alpha y} = \frac{\partial \rho v}{\partial t'}, \qquad \sum_{\alpha=0}^{8} F_\alpha \left(\frac{\xi_{\alpha x}^2 + \xi_{\alpha y}^2}{2} \right) = \frac{\sigma^2}{2} \frac{\partial \rho}{\partial t'}, \tag{3.2b}$$

where t' is the real physical time and t is treated as the pseudo-time for iteration purpose. Similar to the derivation given in [2], multiplying Eq. (2.5) with respect to $\left(1, \xi_\alpha, |\xi_\alpha|^2/2\right)^T$, taking summation over α, and using Eq. (3.2), the following equations are obtained,

$$\frac{\partial \rho}{\partial t'} + \frac{\partial}{\partial t}\left(\sum_\alpha f_\alpha \right) + \frac{\partial \rho u}{\partial x} + \frac{\partial \rho v}{\partial y} = -\frac{1}{\varphi}\left(\sum_\alpha f_\alpha - \rho \right), \tag{3.3a}$$

$$\frac{\partial \rho u}{\partial t'} + \frac{\partial \rho u}{\partial t} + \frac{\partial \rho u^2 + p - \tau_{xx}}{\partial x} + \frac{\partial \rho uv - \tau_{xy}}{\partial y} = \mathcal{O}(\varphi), \tag{3.3b}$$

$$\frac{\partial \rho v}{\partial t'} + \frac{\partial \rho v}{\partial t} + \frac{\partial \rho uv - \tau_{xy}}{\partial x} + \frac{\partial \rho v^2 + p - \tau_{yy}}{\partial y} = \mathcal{O}(\varphi), \tag{3.3c}$$

$$\frac{\partial}{\partial t}\left[\left(p - \frac{\tau_{xx} + \tau_{yy}}{2} \right) + \frac{1}{2}\rho\left(u^2 + v^2\right) \right] + \frac{\sigma^2}{2}\left(\frac{\partial \rho}{\partial t'} + \frac{\partial \rho u}{\partial x} + \frac{\partial \rho v}{\partial y} \right) = \mathcal{O}(\varphi). \tag{3.3d}$$

It should be noted that Eqs. (3.3a)-(3.3d) are obtained only for the case where σ is a constant. For time varying σ as in Eq. (2.8), the pseudo-time terms of Eq. (3.3b), Eq. (3.3c) and Eq. (3.3d) become

$$\sum_\alpha \xi_{\alpha x} \frac{\partial f_\alpha}{\partial t}, \qquad \sum_\alpha \xi_{\alpha y} \frac{\partial f_\alpha}{\partial t}, \qquad \sum_\alpha \left(\frac{{\xi_{\alpha x}}^2 + {\xi_{\alpha y}}^2}{2} \right) \frac{\partial f_\alpha}{\partial t},$$

respectively, because ξ_α is now pseudo-time dependent. After reaching steady state with respect to the pseudo-time t, all pseudo-time terms vanish, irrespective whether σ is a constant or not. Also, σ is no longer varying with pseudo-time at steady state (i.e. becoming a constant). By noting the setting of $\varphi = \Delta t$ in the numerical procedures, Eqs. (3.3b)-(3.3c) and Eq. (3.3d) become the momentum and the continuity equations of the NS equations, respectively, correct to order of Δt, and from Eq. (3.3a) $\sum_\alpha f_\alpha$ will yield ρ.

Unlike conventional LBM where the pressure is assumed to be related to the density by an equation of state, the pressure of the present scheme is calculated by the distribution function in Eq. (2.6b). By this definition of pressure, the square bracket of the first term of Eq. (3.3d) is in fact,

$$\sum_{\alpha=0}^{8} f_\alpha \frac{1}{2}\left(\xi_{\alpha x}^2 + \xi_{\alpha y}^2 \right),$$

which is the kinetic energy due to the lattice velocity. The second bracketed term in Eq. (3.3d) is essentially the rate of change of mass. Therefore Eq. (3.3d) could be viewed

as a pressure-correction formula by balancing the lattice kinetic energy with the virtual compression work [2–6].

A solution for Eq. (3.2) can be obtained by assuming a minimal form for F_α, such that

$$F_\alpha = A_\alpha + \xi_{\alpha x} A x_\alpha + \xi_{\alpha y} A y_\alpha. \tag{3.4}$$

Following the same rules as those used to deduce the coefficients of g_α [1], one possible set of solutions for Eq. (3.4) is

$$A_0 = 0, \qquad A_1 = \frac{1}{4}\frac{\partial \rho}{\partial t'}, \qquad A_2 = 0, \tag{3.5a}$$

$$A x_1 = \frac{1}{2\sigma^2}\frac{\partial \rho u}{\partial t'}, \qquad A x_2 = 0, \tag{3.5b}$$

$$A y_1 = \frac{1}{2\sigma^2}\frac{\partial \rho v}{\partial t'}, \qquad A y_2 = 0. \tag{3.5c}$$

The physical time derivative term can be approximated by any finite difference method and the Euler method is one of the simplest choices,

$$\frac{\partial Z}{\partial t'} = \frac{Z - Z_0}{\Delta t'}, \tag{3.6}$$

where Z is the updated physical quantity (e.g. ρ, ρu, ρv) iterating in pseudo-time, Z_0 is the physical quantity in the previous physical time step and t' is the step size of the physical time. For incompressible flow cases considered previously where density is a constant [2–4], the derivative of density is simply zero.

4 Validation of the time-accurate FDLBM

Two test cases are used to validate the time-accurate FDLBM; they are the Stokes' 2*nd* problem, and an analytical solution of the 2-D incompressible NS equations [14, 15]. In these two validating examples, (x,y) are respectively the horizontal and vertical coordinates and (u,v) are the horizontal and vertical velocity components along x and y, respectively. The convergent criteria for pseudo-time within each physical time step are discussed in detail in the 2-D incompressible NS equations example.

4.1 Stokes 2*nd* problem

In this simulation, the x-axis coincides with an infinitely long flat plate above which is a viscous fluid. The boundary at $y=0$ is oscillating periodically in time such that,

$$u(y=0,t) = \cos nt. \tag{4.1}$$

An exact solution for this problem is given by,

$$u(y,t)=\exp\left(-y\sqrt{\frac{n\mathrm{Re}}{2}}\right)\cos\left(nt-y\sqrt{\frac{n\mathrm{Re}}{2}}\right). \tag{4.2}$$

The domain is bounded by $0\leq(x,y)\leq 1$ in the numerical simulation. Periodic boundary condition is employed at $x=0$ and $x=1$. The calculation is carried out until a transient state is reached. The velocity is normalized by the maximum oscillating speed $\hat{U}$, the axes are normalized by the characteristic length $\hat{L}$, and the time is normalized by $\hat{L}/\hat{U}$. The Reynolds number is defined by $\mathrm{Re}=\hat{\rho}_0\hat{U}\hat{L}/\hat{\mu}$ where $\hat{\rho}_0$ and $\hat{\mu}$ are the dimensional density and viscosity of the fluid. In the calculation $\mathrm{Re}=20$ and, $n=4\pi$ are specified. The relatively weak condition as in Eq. (2.7) for iteration in pseudo-time is employed. Comparisons of the simulations with the analytical solution given in Eq. (4.2) at various t' are shown in Fig. 2. It can be seen that the time-accurate FDLBM simulation is in excellent agreement with the analytical solution at every t' compared.

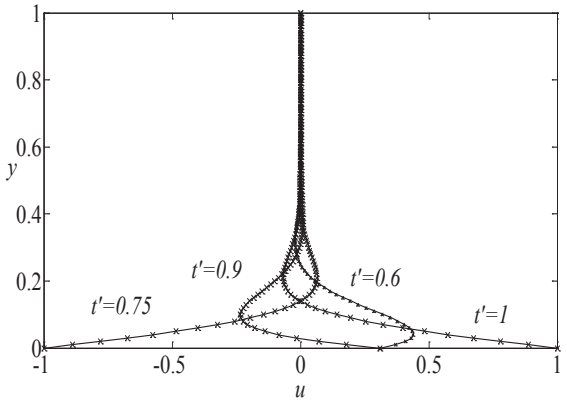

Figure 2: Distribution of the u-velocity along the y-axis at t': "—", exact solution as given by Eq. (4.2); "x", time-accurate FDLBM results.

4.2 2-D analytical solution of incompressible NS equations

An exact solution of the 2-D incompressible NS equations has been given by Kim and Moin [14] (see also [15]). This 2-D unsteady analytical solution can be used as a benchmark to test the time-accurate capability of the unsteady FDLBM scheme used to solve the dimensionless unsteady incompressible NS equations, Eqs. (2.1a)-(2.1c). The analytical solutions as given in [14,15] for p, u and v can be written as

$$p=-\frac{1}{4}(\cos 2x+\cos 2y)\,e^{-4t/\mathrm{Re}}, \tag{4.3a}$$

$$u=-\cos x\sin y e^{-2t/\mathrm{Re}},\qquad v=-\sin x\cos y e^{-2t/\mathrm{Re}}. \tag{4.3b}$$

The computational domain for this calculation is defined by $0 \leq (x,y) \leq \pi$. The initial and boundary conditions are identical to those specified for the exact solution. Other numerical parameters are given by $\rho = 1$, $\sigma = 5$, $\Delta t = \Delta t' = 1e-4$, $\Delta x = \pi/100$.

Effects of the different convergent criterion on the simulation results are analyzed in this example. As a first attempt, the weaker condition, Eq. (2.7), used in the previous example is employed. Also, a fixed value for σ, instead of a dynamic form suggested in Eq. (2.8) is used. In fact, for this problem, even when the dynamic form is employed, the σ value is found to be almost constant. In addition, the following criteria have also been examined;

$$\max \|\partial(p)\|_{\text{whole domain}} \leq \frac{\Delta t^2 \sigma^2}{2}, \tag{4.4a}$$

$$\max \|\partial(u)\|_{\text{whole domain}} \leq \Delta t^2, \tag{4.4b}$$

$$\max \|\partial(v)\|_{\text{whole domain}} \leq \Delta t^2. \tag{4.4c}$$

Table 1 compares the maximum error norm between the numerical solution and the exact solution over the whole spatial and temporal domain. Since the Euler method is used to discretize the derivative of the physical time, the accuracy of the scheme is estimated to be first order in both physical and pseudo times, i.e., $\mathcal{O}(\phi = t = t' = 1e-4)$. Further, the Lax-Wendroff scheme is used in the streaming step, therefore, the scheme is only second order accurate in space, i.e., $\mathcal{O}(\Delta x^2 = (\pi/100)^2 \approx 9.870e-4 \approx 1e-3)$. In Table 1, the time-accurate FDLBM results of the flow velocities for all Reynolds numbers considered are in excellent agreement with exact solutions. On the other hand, the pressure results for the cases where Re is small (Re = 1 and 10) are not very good. This is because the use of the pseudo-time iteration criterion, Eq. (2.7), can only ensure mass conservation up to $\mathcal{O}(\Delta t)$, i.e.

$$\frac{\partial \rho}{\partial t'} + \frac{\partial \rho u}{\partial x} + \frac{\partial \rho v}{\partial y} = \mathcal{O}(\Delta t). \tag{4.5}$$

However, the steadiness of the complete temporal term, which is defined by the sum of the pressure, kinetic energy and the normal stresses, is in fact bounded by the weaker condition (see Eq. (2.7)). For Newtonian fluid, the sum of the normal stresses is propor-

Table 1: Maximum error norm for the unsteady 2-D problem using convergent criteria Eqs. (2.7) and (4.4).

	$\max\|\Delta u\|$	$\max\|\Delta v\|$	$\max\|\Delta p\|$
Re = 1	7.7537e-5	7.3868e-5	2.6735e-2
Re = 10	1.9189e-4	1.9974e-4	1.6584e-2
Re = 100	5.5622e-4	4.8894e-4	2.6660e-3
Re = 1000	1.0115e-3	6.6121e-4	2.5661e-3
Re = 10000	1.1474e-3	7.0179e-4	2.6789e-3

tional to the divergence condition,

$$\tau_{xx}+\tau_{yy}=\frac{1}{\mathrm{Re}}\left(\frac{\partial u}{\partial x}+\frac{\partial v}{\partial y}\right). \tag{4.6}$$

Hence; without sufficient accuracy in the steadiness of the pressure term, the error due to the divergence condition will directly carry over to the pressure and this situation is even worse for smaller Re, because at small Re the viscous terms are comparatively more important.

Further investigation has been carried out by repeating the calculation with the same numerical and physical parameters but using the following two set of stronger criteria

$$\max\left\|\partial\left(p+\frac{1}{2}\rho|\vec{u}|^2-\frac{\tau_{xx}+\tau_{yy}}{2}\right)\right\|_{\text{whole domain}}\leq\frac{\Delta t^2\sigma^2}{10}, \tag{4.7a}$$

$$\max\|\partial(p)\|_{\text{whole domain}}\leq\frac{\Delta t^2\sigma^2}{10}, \tag{4.7b}$$

and

$$\max\left\|\partial\left(p+\frac{1}{2}\rho|\vec{u}|^2-\frac{\tau_{xx}+\tau_{yy}}{2}\right)\right\|_{\text{whole domain}}\leq\Delta t^2, \tag{4.8a}$$

$$\max\|\partial(p)\|_{\text{whole domain}}\leq\Delta t^2, \tag{4.8b}$$

while the steadiness of the flow velocity is still given by Eqs. (4.4b)-(4.4c). The criteria of $\max\left\|\partial\left(p+\rho|\vec{u}|^2/2-\left(\tau_{xx}+\tau_{yy}\right)/2\right)\right\|$ and $\max\|\partial(p)\|$ are changed simultaneously in the analysis because it is found that their convergent behaviors are almost the same. Since the value of σ is fixed at 5 in the calculation, $\Delta t^2\sigma^2/10=2.5\Delta t^2$ can be deduced from Eqs. (4.7a)-(4.7b). Only the cases with small Re (Re = 1 and 10) are repeated and the results are shown in Tables 2 and Tables 3 for comparison. The pressure results are much improved when the stronger convergent criteria are used to control the pseudo-time iteration. Hence, it is inferred that the convergent criteria given in Eqs. (4.8a)-(4.8b) and

Table 2: Maximum error norm for the unsteady 2-D problem using convergent criteria Eqs. (4.7) and (4.4b)-(4.4c).

	$\max\|\Delta u\|$	$\max\|\Delta v\|$	$\max\|\Delta p\|$
Re = 1	2.9554e-5	3.2069e-5	4.6075e-3
Re = 10	1.7692e-4	1.9266e-4	8.2444e-3

Table 3: Maximum error norm for the unsteady 2-D problem using convergent criteria Eqs. (4.8) and (4.4b)-(4.4c).

	$\max\|\Delta u\|$	$\max\|\Delta v\|$	$\max\|\Delta p\|$
Re = 1	2.5807e-5	2.9241e-5	2.0033e-3
Re = 10	1.7646e-4	1.9032e-4	2.5075e-3

Eqs. (4.4b)-(4.4c) are suitable for most problems. The convergent criteria can be relaxed as Re increases if computational time is a consideration.

5 Model blood flow problem – pulsating flow in a constricted tube

Before simulating a pulsating unsteady flow through a constricted tube, an unsteady entrance flow development in a straight tube as previously examined by He and Ku [16] is investigated. Successful simulation of an unsteady entrance flow is important for blood flow simulation studies because numerous blood flow problems are of the entrance flow type, e.g., flow in the aortic arch or near the origins of arterial branches. After verifying the entrance flow development with the data of [16], pulsating unsteady flow through a constricted tube is simulated using the time-accurate FDLBM/IB. Two examples with Newtonian fluid are presented in detail; one for small Re and small Womersley number, and another for large Re and large Womersley number. This is then followed by a case of non-Newtonian fluid (with the CY model). That way, a direct assessment of the effect of non-Newtonian fluid on the pulsating constricted flow could be carried out by comparing the pressure drop.

The same dimensionless parameters as in Eq. (2.3) are employed except that time is now normalized as $t=\hat{t}/\hat{T}$, where $\hat{T}$ is the period of the upstream pulsation. The governing equations are the unsteady incompressible NS equations and, after normalization, they can be written as

$$\frac{\partial u}{\partial x}+\frac{\partial v}{\partial y}+\frac{v}{y}=0, \tag{5.1a}$$

$$\frac{\alpha^2}{2\pi\mathrm{Re}}\frac{\partial u}{\partial t}+\frac{\partial u^2}{\partial x}+\frac{\partial uv}{\partial y}+\frac{uv}{y}=-\frac{\partial p}{\partial x}+\frac{\partial \tau_{xx}}{\partial x}+\frac{\partial \tau_{xy}}{\partial y}+\frac{\tau_{xy}}{y}, \tag{5.1b}$$

$$\frac{\alpha^2}{2\pi\mathrm{Re}}\frac{\partial v}{\partial t}+\frac{\partial uv}{\partial x}+\frac{\partial v^2}{\partial y}+\frac{v^2}{y}=-\frac{\partial p}{\partial y}+\frac{\partial \tau_{xy}}{\partial x}+\frac{\partial \tau_{yy}}{\partial y}+\frac{\tau_{yy}}{y}, \tag{5.1c}$$

where Re is the Reynolds number and α is the Womersley parameter defined as

$$\alpha=\hat{R}_0\sqrt{\frac{2\pi}{\hat{T}}/\frac{\hat{\mu}_0}{\hat{\rho}_0}}. \tag{5.2}$$

The coefficient of the unsteady term $\alpha^2/(2\pi\mathrm{Re})=\left(\hat{R}_0/\hat{U}_0\right)/\hat{T}$ is in fact the ratio of the characteristic time for steady Poiseuille flow to the period of upstream pulsation which characterizes the unsteadiness. At the centerline ($y=0$), a reflective boundary given by

$$\frac{\partial u}{\partial y}=0, \qquad v=0, \qquad \frac{\partial p}{\partial y}=0 \tag{5.3}$$

is set and no slip condition is specified at the wall ($y=1$). A prescribed velocity profile is specified at the entrance and a fully developed condition is assumed at the downstream exit, i.e.,

$$\frac{\partial u}{\partial x}=0, \qquad v=0. \tag{5.4}$$

The lattice Boltzmann equation, Eq. (3.1), in the time-accurate FDLBM is used to recover the set of NS equations as given in Eqs. (5.1)-(5.2).

5.1 Unsteady developing entrance flow

An unsteady entrance flow development in a straight tube is simulated; the prescribed upstream velocity is given by

$$u=1+A\sin(2\pi t), \qquad v=0, \tag{5.5}$$

where A is the amplitude of the pulsation. For this case $A=1$ is specified. The initial condition is assumed to be given by a uniform flow (specified everywhere except the wall where a no-slip condition is imposed). For simulation purpose, $\mathrm{Re}=100$ is chosen, which corresponds to the same condition of $\mathrm{Re}_{\mathrm{mean}}=200$ in [16]. Thus, current results can be directly compared with those given in [16], and a validation of the time-accurate FDLBM can be made.

Time development of the flow at the centerline for the case $\alpha=12.5$ is shown in Fig. 3. It is noted that time is normalized by the period of the pulsation so that each unit of time corresponds to one cycle. Fig. 3 shows that four cycles is required for a transient flow to be developed. The development of the flow along the x-direction at different phase angles is shown in Fig. 4. Other simulation data are available for this case (where the data was obtained by numerically solving the unsteady NS equations [16]). The time-accurate FDLBM result of the calculated time-averaged value and amplitude of the centerline u-velocity is compared with the data of [16] in Fig. 5. In addition, the fully developed u-velocity profile at a downstream location is compared with the data of [16] in Fig. 6;

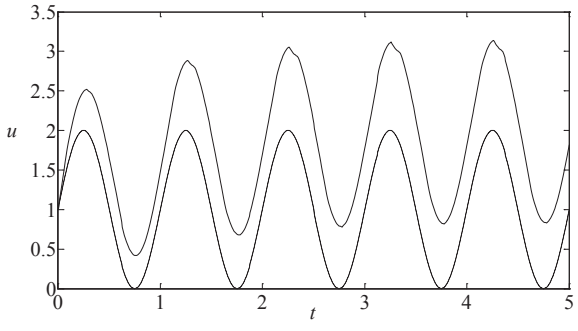

Figure 3: Centerline entrance flow development of u versus t: "– –" upstream; "—" downstream.

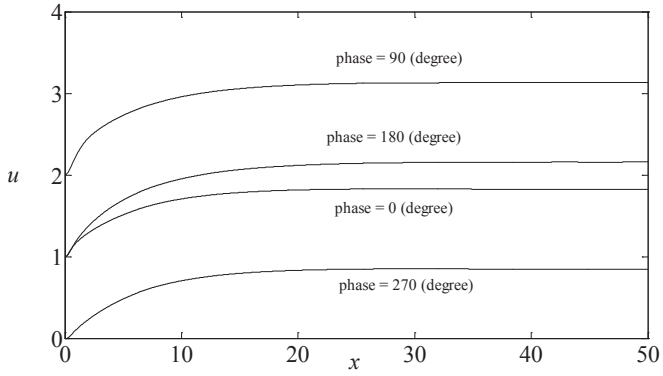

Figure 4: Centerline entrance flow development of u versus x at different phase angle.

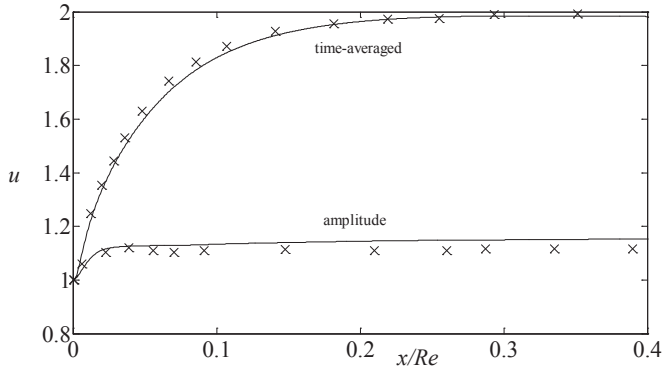

Figure 5: Comparison of the time-averaged value and amplitude of u along x-axis: "—", time-accurate FDLBM result; "x", data of [16].

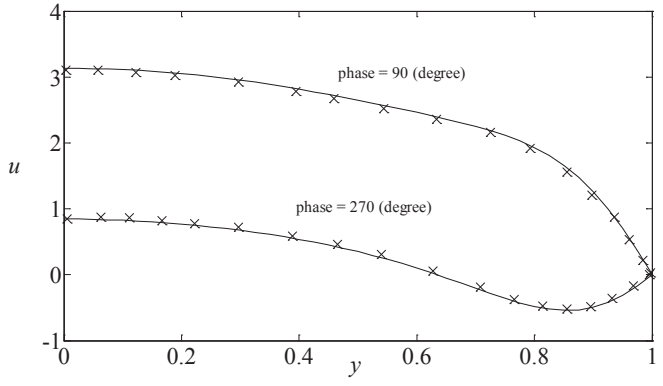

Figure 6: Comparison of the fully developed u-velocity profile at a downstream location: "—" time-accurate FDLBM result; "x", data of [16].

this is essentially the Womersley profile. It can be seen that the current time-accurate FDLBM simulations are in excellent agreement with the numerical results of [16]; thus validating the present time-accurate FDLBM approach.

5.2 Pulsating Newtonian flow in a constricted tube

Having verified the accuracy of the time-accurate FDLBM by an unsteady developing entrance flow, the next step is to assess the performance of the time-accurate FDLBM/IB in its simulation of a pulsating unsteady flow through a constricted tube. A constriction model designated as M02 is chosen for investigation; this model has the following properties, $\alpha_1 = 0.5$, $X_0 = 2$ and an area reduction of 75%. As a first attempt, a low Re number is studied. In this case, the physical parameters are specified as $\mathrm{Re} = 50$ and $\alpha = 2.5$. The prescribed upstream velocity is

$$u = \left(1 - y^2\right)\ [1 + A\sin\left(2\pi t\right)], \qquad v = 0, \tag{5.6}$$

where $A = 0.5$ is assumed. The initial condition is chosen to be the steady state solution calculated under the same physical and geometric conditions, so that at $t = 0$, the upstream velocity profile is exactly matched with the initial condition. The calculation is carried out for 5 cycles so that a transient state is ensured. The periodic behavior at transient of the u-velocity and pressure profile is shown in Figs. 7a and 7b, respectively. In Figs. 8a-d, the streamlines are plotted at different phase angles defined as $\theta = 2\pi t/360$. The vortex structure is similar to that of the steady case, but it is clear that the size of the vortex behind the constriction is changing within a cycle.

A case with larger Re, larger Womersley parameter, and larger amplitude of velocity fluctuation at upstream is also examined. The physical parameters chosen are $\mathrm{Re} = 100$, $\alpha = 12.5$ and $A = 1.0$. With this upstream setting, the upstream velocity is still positive but can be zero at $\theta = 180^\circ$. The vortex structure at transient for eight different θ is more complex and is shown in Fig. 9. More than one vortex can be observed behind the constriction which is different from the smaller Re case (Fig. 8). The development of the vortices within one cycle is shown in Fig. 9. Successful capture of the pulsatile behavior of the constricted tube flow by the current time-accurate FDLBM/IB and the interesting change of the vortex shown encourage further study of the pulsatile constricted flow for different Re and α and for 3-D flow where the constriction surface can vary with time and flow. These cases are not treated in the present paper. Instead, a non-Newtonian fluid flow through a constricted tube is studied in order to assess the effect of non-Newtonian fluid effect on the constricted flow behavior.

5.3 Pulsating non-Newtonian flow in a constricted tube

In this section, the ability of the scheme to simulate pulsating non-Newtonian fluid flow through constricted tube is demonstrated. Again the constriction model designated as M02 is chosen for investigation. The only difference between the current case and those

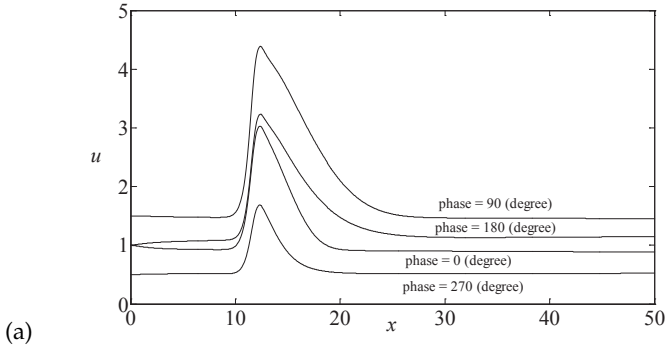

(a)

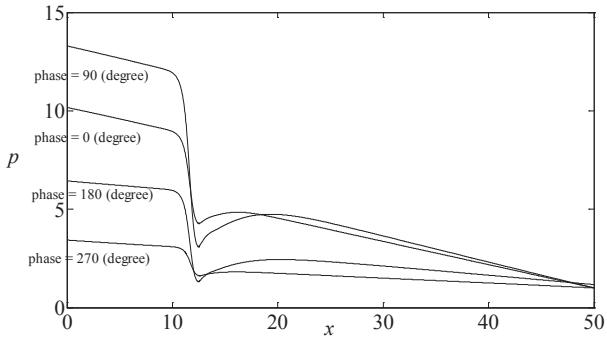

(b)

Figure 7: Pulsating u-velocity and pressure profile at centerline for model M02 at $\mathrm{Re}=50$ and $\alpha=2.5$: (a) u-profile; (b) p-profile.

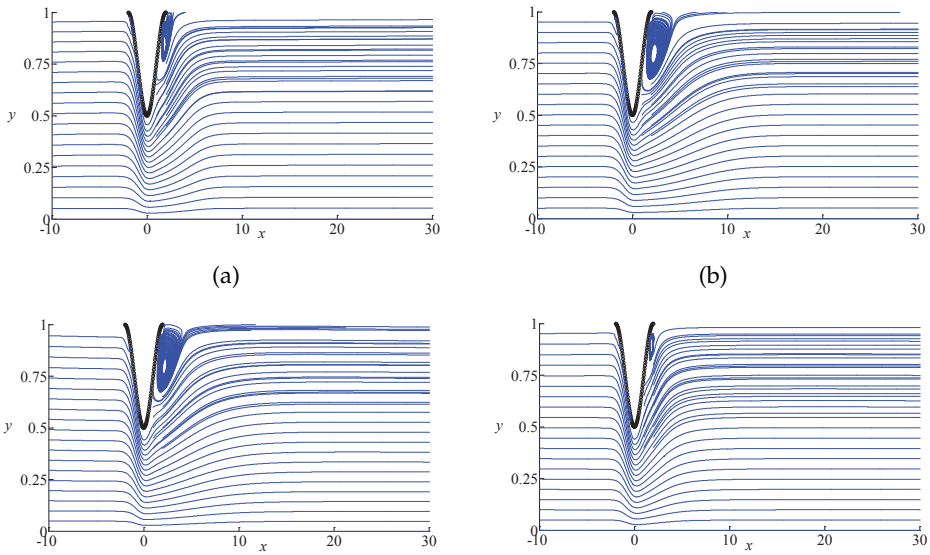

(a) (b) (c) (d)

Figure 8: Streamline plots at different phase angle θ for model M02 with $\mathrm{Re}=50$ and $\alpha=2.5$: (a) $\theta=0^\circ$; (b) $\theta=90^\circ$; (c) $\theta=180^\circ$; (d) $\theta=270^\circ$.

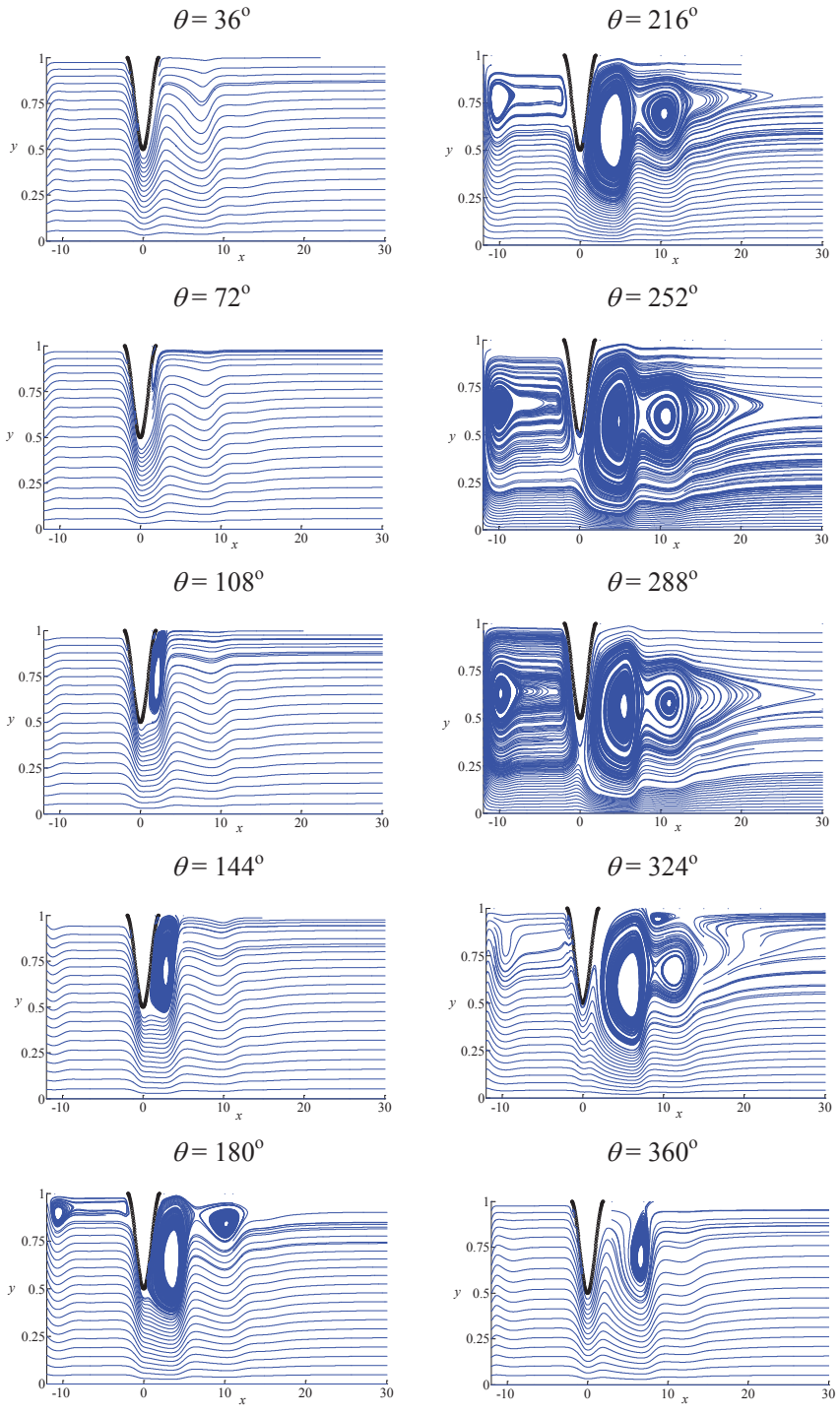

Figure 9: Streamline plots at different phase angle θ for model M02 with $\mathrm{Re}=100$ and $\alpha=12.5$.

of the Newtonian fluid flow cases is in the viscosity model. The non-Newtonian Carreau-Yasuda (CY) viscosity model is chosen to replicate the shear thinning phenomena of blood flow as discussed in [1]. Detailed description of the CY model can be found in [1, 17–19]. The viscosity coefficient is no longer constant. In dimensionless form, μ can be expressed as follows,

$$\mu=\frac{1}{\mathrm{Re}_\infty}+\left(\frac{1}{\mathrm{Re}_z}-\frac{1}{\mathrm{Re}_\infty}\right)\left[1+(\lambda\,|\dot{\gamma}|)^a\right]^{\frac{n-1}{a}}. \tag{5.7}$$

The scalar measure of the rate of deformation $|\dot{\gamma}|$ is as defined in [19], i.e.,

$$|\dot{\gamma}|=\sqrt{\frac{1}{2}\sum_i\sum_j\dot{\gamma}_{ij}\dot{\gamma}_{ji}}=\sqrt{2\left(\frac{\partial u}{\partial x}\right)^2+\left(\frac{\partial u}{\partial y}+\frac{\partial v}{\partial x}\right)^2+2\left(\frac{\partial v}{\partial y}\right)^2}\qquad\text{for 2D,} \tag{5.8}$$

and the two specific Reynolds numbers corresponding to the viscosity at zero ($\hat{\mu}_z$) and infinite ($\hat{\mu}_\infty$) shear rate are defined as

$$\mathrm{Re}_z=\frac{\hat{\rho}_0\hat{U}_0\hat{R}_0}{\hat{\mu}_z},\qquad \mathrm{Re}_\infty=\frac{\hat{\rho}_0\hat{U}_0\hat{R}_0}{\hat{\mu}_\infty}. \tag{5.9}$$

The physical parameters employed in the calculation are $a=0.644$, $n=0.392$, $\mathrm{Re}_z=25.324$, $\mathrm{Re}_\infty=253.24$, $\lambda=14.59$ [1] and $\alpha=2.5$ where α, the Womersley number, is normalized by $\hat{\mu}_z$. The prescribed upstream velocity is the same as that given by Eq. (5.6) with $A=0.5$ and all other boundary conditions are identical to the Newtonian cases. The vortex structure within a cycle at transient is shown in Fig. 10. Similar to the Newtonian cases, the size of the vortex is changing periodically except the vortex is larger on average. This result is similar to that of the steady case [1].

A wealth of information is available from these Newtonian and non-Newtonian fluid flow simulations. The present paper would become too long if these data were fully analyzed to decipher the characteristics of this model blood flow problem. It is more appropriate to devote a separate paper to a study of these characteristics. However, one important parameter that is quite relevant to the understanding of stenosis could be extracted from these simulations. This parameter is the pressure drop $\delta\hat{p}$ given by the flow with and without a constriction. Defining $\delta\hat{p}$ as the difference between the pressure far downstream of the constriction and the pressure at the same location calculated without the constriction, the mean pressure drop $\delta\hat{p}_m$ can be calculated from

$$\delta\hat{p}_m=\frac{1}{\hat{T}}\int_{\hat{t}_0}^{\hat{t}_0+\hat{T}}\delta\hat{p}\,d\hat{t}, \tag{5.10}$$

where $\delta\hat{p}$ is by nature fluctuating (periodically) as a consequence of the inlet flow. In order to assess the behavior of $\delta\hat{p}_m$, several more cases are calculated; the conditions for these cases are tabulated in Table 4 together with the calculated dimensionless mean pressure drop δp_m (normalized by $\hat{\rho}_0\hat{U}_0^2$) for these cases.

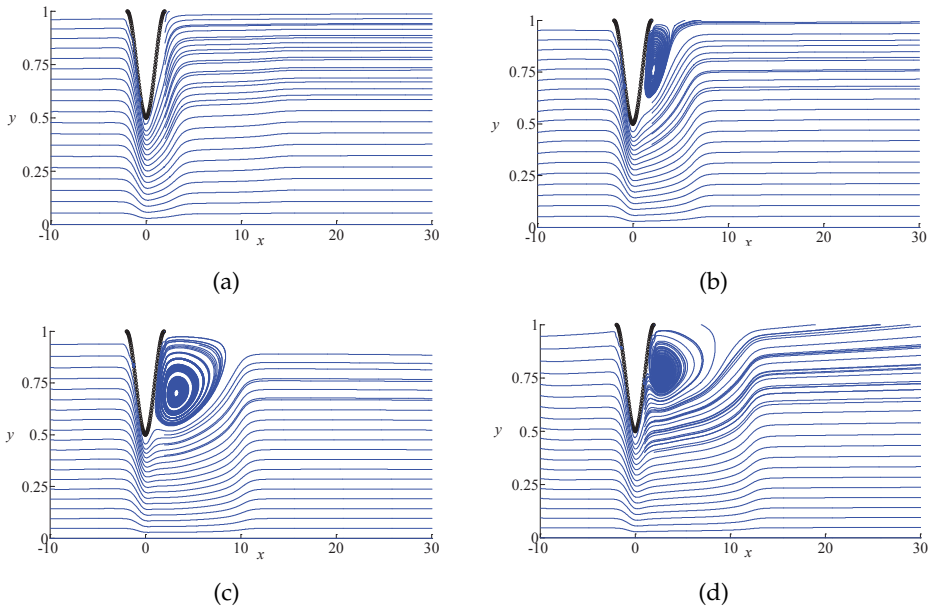

Figure 10: Streamline plots at different phase angle θ for M02 with CY model and $\alpha=2.5$: (a) $\theta=0^\circ$; (b) $\theta=90^\circ$; (c) $\theta=180^\circ$; (d) $\theta=270^\circ$.

Table 4: Mean pressure drop δp_m for various cases of simulated Newtonian and non-Newtonian fluid flow in constricted pipes.

Case	Upstream Condition given by	δp_m				
		A	α	Re=50	Re=100	CY Model
1	Steady flow [1]	0	0	2.9333	2.0818	1.5063
2	Eq. (5.6)	0.5	2.5	3.1562	2.2881	1.7035
3	Eq. (5.6)	1.0	2.5	3.7776	2.8042	2.2244
4	Eq. (5.6)	1.0	12.5		3.5362	

From these results, it can be seen that, for Newtonian fluid, the mean pressure drops are larger than those for the steady cases. Further, when the upstream fluctuation amplitude A increases, i.e., using $A=1.0$ instead of $A=0.5$ for upstream condition, the mean pressure drop also increases. Larger α leads to greater pressure drop while larger Re gives rise to a smaller pressure drop. However, the mean pressure drop δp_m decreases as Re is increased from 50 to 100. The behavior for non-Newtonian (CY model) fluid in pulsatile flow is similar to that of the steady case. The mean pressure drops are smaller than those for Newtonian cases, and they are also smaller than that for the steady flow case.

The coefficient of the unsteady term in Eqs. (5.1)-(5.2) is in fact the ratio of the characteristic time for steady Poiseuille flow to the period of upstream pulsation that characterizes the unsteadiness. Numerically, it appears that this ratio plays a more dominant

role than α, the Womersley number. Since this ratio is given by $\alpha^2/(2\pi\text{Re})$, its value for Case 2 and 3 listed in Table 4 can be calculated as 0.0199 and 0.00995 for Re = 50 and 100, respectively. For Case 4, the corresponding $\alpha^2/(2\pi\text{Re})$ values are 0.4974 and 0.2487, respectively. Therefore, it can be seen that fixing Re and doubling α, $\alpha^2/(2\pi\text{Re})$ is increased by a factor of 4. On the other hand, fixing α and doubling Re, $\alpha^2/(2\pi\text{Re})$ is decreased by half. Convergent difficulty has been found when calculating Case 4 with Re = 50 and α=12.5. This is not surprising because $\alpha^2/(2\pi\text{Re})$ increases by 25 times compared to Case 2 and 3 with Re=50 and α=2.5. Consequently, the simulation for Case 4 with α=12.5 and Re = 50 is very sensitive to the initial conditions specified. Attempts are being made to investigate whether this case can be solved using a finer grid, or whether a transition to turbulent flow has occurred. If transition has indeed occurred, the axisymmetric laminar model assumed here is no longer valid. In non-Newtonian fluid, viscosity is not constant; thus leading to varying Re and $\alpha^2/(2\pi\text{Re})$ in the course of the simulation. The variation of $\alpha^2/(2\pi\text{Re})$ in the calculation compounds the difficulty encountered in the simulation of Case 4 assuming a CY model for the non-Newtonian fluid. These numerical attempts, therefore, suggest that the time ratio $\alpha^2/(2\pi\text{Re})$ is a more important parameter than α in the numerical simulation of pulsatile flow through constricted tubes.

6 Conclusions

The first objective of this paper is to extend the steady FDLBM [2–4] to a time-accurate scheme. Once accomplished, the second objective is to use the same methodology to extend the steady FDLBM/IB [1] method to a time-accurate one so that the time-accurate FDLBM/IB numerical scheme can be used to treat axisymmetric pulsating flow with complex wall boundaries. The first objective has been successfully accomplished; the effectiveness and accuracy of the time-accurate FDLBM scheme is fully demonstrated. This is evident by the excellent agreement between current results and those given by known analytical solution and deduced from well tested numerical simulations of the NS equations for 2-D unsteady flow and unsteady entrance flow development in a straight tube. The time-accurate methodology is extended to the FDLBM/IB scheme [1] and the resultant numerical algorithm is used to investigate a model blood flow problem, i.e., an axisymmetric pulsating flow in a constricted tube with 75% area reduction at different sets of Re and α for both Newtonian fluid and non-Newtonian fluid (CY model). These models are similar to those used by previous researchers to simulate blood flow through stenotic arteries. The results show that the flow behind the constriction is dependent on both Re and α. For example, at low Re and α, only one vortex is observed, while more than one vortices are calculated for the higher Re and α case examined. Furthermore, it is found that non-Newtonian fluid gives rise to a smaller pressure drop compared to Newtonian fluid under the same flow conditions. Through these examples, the ability and performance of the time-accurate FDLBM/IB numerical scheme is validated. Thus, the algorithm is ready for extension to treat 3-D flow of non-Newtonian fluid through

a constricted tube where the tube wall and the constriction surface can be elastic and fluid-structure interaction plays a key role in the flow behavior.

Acknowledgments

SCF gratefully acknowledges funding support in the form of a PhD studentship awarded him by the Hong Kong Polytechnic University. RMCS acknowledges support received as Co-PI from the NSF Grant CBET-0854411 awarded to New Mexico State University.

References

[1] Fu, S. C., Leung, W. W. F. and So, R. M. C., 2013, A Lattice Boltzmann and Immersed Boundary Scheme for Model Blood Flow in Constricted Pipes: Part 1 - Steady Flow, Communications in Computational Physics, 14(1), 126-152.
[2] Fu, S. C., Leung, W. W. F. and So, R. M. C., 2009, A Lattice Boltzmann Based Numerical Scheme for Microchannel Flows, Journal of Fluids Engineering, 131(August), Paper No. 081401(11 pages).
[3] Fu, S. C. and So, R. M. C., 2009, Modeled Boltzmann Equation and the Constant Density Assumption, AIAA Journal, 47(12), 3038-3042.
[4] Fu, S. C., So, R. M. C. and Leung, W. W. F., 2010, Stochastic Finite Difference Lattice Boltzmann Method for Steady Incompressible Flows, Journal of Computational Physics 229(17), 6084-6103.
[5] Fu, S. C., So, R. M. C. and Leung, W. W. F., 2011, A Discrete Flux Scheme for Aerodynamic and Hydrodynamic Flows, Communications in Computational Physics 9(5), 1257-1283.
[6] Fu, S. C., 2011, Numerical Simulation of Blood Flow in Stenotic Arteries, PhD thesis, Mechanical Engineering Department, The Hong Kong Polytechnic University, Hung Hom, Hong Kong.
[7] Peskin, C. S., 1977, Numerical Analysis of Blood Flow in the Heart, Journal of Computational Physics, 25(3), 220-252.
[8] Mittal, R. and Iaccarino G., 2005, Immersed Boundary Methods, Annual Review of Fluid Mechanics, 37, 239-261.
[9] Deshpande, M. D., Giddens, D. P. and Mabon, R. F., 1976, Steady Laminar Flow Through Modeled Vascular Stenoses, Journal of Biomechanics, 9(4), 165-174.
[10] Rastogi, A. K., 1984, Hydrodynamics in Tubes Perturbed by Curvilinear Obstructions, Journal of Fluids Engineering, 106(3), 262-269.
[11] Beyer, R. P. and Leveque, R. J., 1992, Analysis of a One-Dimensional Model for the Immersed Boundary Method, SIAM Journal on Numerical Analysis, 29(2), 332-364.
[12] Lai, M. C. and Peskin, C. S., 2000, An Immersed Boundary Method with Formal Second-Order Accuracy and Reduced Numerical Viscosity, Journal of Computational Physics, 160(2), 705-719.
[13] Tannehill, J. C., Anderson, D. A. and Pletcher, R. H., 1997, Computational Fluid Mechanics and Heat Transfer, 2nd ed., Taylor & Francis, Washington, D.C., Chap. 9, pp. 649-776.
[14] Kim, J. and Moin, P., 1985, Application of a Fractional-Step Method to Incompressible Navier-Stokes Equations, Journal of Computational Physics 59, 308-323.

[15] Rogers, S. E., Kwak, D. and Kiris, C., 1989, Numerical Solution of the Incompressible Navier-Stokes Equations for Steady-State and Time-dependent Problems, AIAA paper 89-0463, Reno, Nevada.
[16] He, X. and Ku, D. N., 1994, Unsteady Entrance Flow Development in a Straight Tube, Journal of Biomechanical Engineering, 116, 355-360.
[17] Wang, D., and Bernsdorf, J., 2009, Lattice Boltzmann Simulation of Steady Non-Newtonian Blood Flow in a 3D Generic Stenosis Case, Computer and Mathematics with Applications, 58(5), pp. 1030-1034.
[18] Gijsen, F. J. H., van de Vosse, F. N. and Janssen, J. D., 1999, The Influence of the Non-Newtonian Properties of Blood on the Flow in Large Arteries: Steady Flow in a Carotid Bifurcation Model, Journal of Biomechanics, 32, pp. 601-608.
[19] Bird, R. B., Armstrong, R. C. and Hassager, O., 1987, Dynamics of Polymeric Liquids, Vol. 1, 2nd ed., Wiley, New York, p. 171.